NATIONAL ADVISORY COMMITTEE FOR AERONAUTICS

TECHNICAL NOTE 2011

SPANWISE LOADING FOR WINGS AND CONTROL SURFACES OF LOW ASPECT RATIO

By John DeYoung

Ames Aeronautical Laboratory
Moffett Field, Calif.

Washington
January 1950

NATIONAL ADVISORY COMMITTEE FOR AERONAUTICS

TECHNICAL NOTE 2011

SPANWISE LOADING FOR WINGS AND CONTROL SURFACES OF LOW ASPECT RATIO

zero aspect ratio wing!

By John DeYoung

SUMMARY

The boundary conditions for low-aspect-ratio wings are approximately satisfied by a two-dimensional vortex sheet that extends to infinity fore and aft. Since the downwash is constant fore and aft, the boundary condition that no flow passes through the wing or flat plate is satisfied simply by the familiar downwash integral used in line-theory loading methods. A theory is developed herein, based on the foregoing principle which (for small aerodynamic angles and for plan forms that have all points of the trailing edge at or behind the upstream line of maximum span) will predict the spanwise loading due to arbitrary spanwise angle-of-attack distribution, including (1) uniform angle of attack, (2) that induced by rolling, (3) spanwise variation of twist or camber, and (4) that due to deflection of arbitrary control surfaces of low aspect ratio. The spanwise loadings are independent of the plan forms considered.

It is found for plan forms having unswept trailing edges that the spanwise loading distribution depends only on the slope of the region at the wing trailing edge. Thus, in the limit case of zero aspect ratio of wings and control surfaces, the spanwise loading is independent of the position of the hinge line along the wing chord. In addition, the total loading due to any chordwise camber distribution depends only on the slope at the wing trailing edge, provided the curvature at the trailing edge is small as compared with the slope.

From considerations of the linearized-compressible-flow equation, the aerodynamic values given by zero-aspect-ratio theory are also those of moderate-aspect-ratio wings at the speed of sound. The results are applicable for low values of the product of the Prandtl-Glauert compressibility parameter and aspect ratio.

INTRODUCTION

The aerodynamic characteristics of pointed-wing plan forms with aspect ratio approaching zero have been considered by R. T. Jones (reference 1) and extended by H. S. Ribner (reference 2) to include all

the stability derivatives for the pointed triangular wing. The triangular wing of references 1 and 2 is treated on the assumption that the flow potential in planes at right angles to the long axis of the airfoil is similar to the corresponding two-dimensional potential. This theory gives the surface loading for the flat plate and can be extended to the computation of all the important aerodynamic characteristics.

Reference 3 obtains surface loadings for swept wings with the linearized-compressible-flow equation of supersonic theory, which, at the speed of sound, results in equivalent plan forms that have zero aspect ratio. Reference 3 gives the lift coefficient and induced drag for a range of constant-chord swept wings, which results are applicable for low-aspect-ratio swept wings throughout the speed range and moderate-aspect-ratio wings at the speed of sound.

A theory for the rectangular wing of low aspect ratio has been given by W. Bollay (reference 4). This work considers the flow leaving the side edges of the plate at all angles of attack and thus approximates the early separation occurring on blunt plan forms. The results indicate that lift varies nonlinearly with angle of attack as aspect ratio becomes small. It can be assumed by the theory of reference 1 that the flow sticks to the plate, an assumption which is more valid for pointed than for blunt plan forms since loading is continually generated on the swept leading edge. Thus, lift varies linearly with angle of attack for a greater range of angle of attack for the pointed than for the blunt plan form.

There has been, up to the present, no published work presenting control-surface and twist effects for low-aspect-ratio wings or for moderate-aspect-ratio wings at sonic speeds. The primary purpose of the present report is to extend the theory of reference 1 to provide a means of predicting aerodynamic characteristics resulting from the deflection of arbitrary control surfaces of low aspect ratio on low-aspect-ratio wings. Since the linearized-compressible-flow equation indicates that low values of the product of the Prandtl-Glauert parameter and aspect ratio are satisfied by low-aspect-ratio theory, the results will be applicable throughout the speed range for low-aspect-ratio wings and at sonic speeds for moderate-aspect-ratio wings.

SYMBOLS

A	aspect ratio (b^2/S)
a_n	coefficients of the trigonometric series for spanwise loading
b	wing span measured perpendicular to the plane of symmetry, feet

c	wing chord, feet[1]
C_{L_α}	lift due to angle of attack $\left(\frac{\partial C_L}{\partial \alpha}\right)$, per radian
C_{L_δ}	lift due to control-surface deflection $\left(\frac{\partial C_L}{\partial \delta}\right)$, per radian
C_{l_p}	rolling moment due to rolling $\left[\frac{\partial C_l}{\partial (pb/2V)}\right]$, per radian
C_{l_δ}	rolling moment due to control-surface deflection $\left(\frac{\partial C_l}{\partial \delta}\right)$, per radian
C_L	wing lift coefficient $\left(\frac{\text{total lift}}{qS}\right)$
C_l	rolling-moment coefficient $\left(\frac{\text{rolling moment}}{qSb}\right)$
c_l	local lift coefficient $\left(\frac{\text{local lift}}{qc}\right)$
C_{D_i}	induced drag coefficient $\left(\frac{\text{induced drag}}{qS}\right)$
G	spanwise loading coefficient $\left(\frac{c_l c}{2b}\right)$ or dimensionless circulation $\left(\frac{\Gamma}{bV}\right)$
M	Mach number
n	integer coefficients of loading series
p	rate of rolling, radians per second
$\frac{pb}{2V}$	rolling helix angle, radians
q	free-stream dynamic pressure, pounds per square foot
S	wing area, square feet
V	free-stream velocity, feet per second

[1]Quantities measured parallel to the plane of symmetry.

w	induced velocity, normal to the wing, positive for downwash, feet per second
$\bar{y}$	lateral coordinate pertaining to loading, measured from wing root perpendicular to plane of symmetry, feet
y	lateral coordinate pertaining to downwash, feet
α	constant spanwise angle of attack, radians[1]
$\alpha(\varphi)$	variable spanwise angle of attack, radians[1]
α_r	wing root angle of attack when total lift equals zero, radians[1]
β	compressibility parameter $\left(\sqrt{\lvert 1-M^2 \rvert}\right)$
Γ	spanwise circulation, feet squared per second
δ_1,δ_2	arbitrary control-surface angles for each semispan, radians[1]
$\epsilon(\varphi)$	wing twist relative to root chord, radians[1]
$\bar{\eta}$	dimensionless lateral coordinate pertaining to loading $\left(\frac{\bar{y}}{b/2}\right)$
η	dimensionless lateral coordinate pertaining to downwash $\left(\frac{y}{b/2}\right)$
$\eta_{c.p.}$	semispanwise center-of-pressure location
θ	parameter defining position of control-surface spanwise edge, radians
λ	taper ratio $\left(\frac{\text{tip chord}}{\text{root chord}}\right)$
Λ_β	sweep-angle parameter, positive for sweepback $\left(\tan^{-1}\frac{\tan\Lambda}{\beta}\right)$, degrees

Subscripts

ν	integer pertaining to span station

[1]See footnote 1, page 3

a ailerons

f flaps

THEORY FOR WINGS OF ZERO ASPECT RATIO

Plan-Form Range and Boundary Conditions

The surface loading on a wing can be represented by a vortex sheet. The vortex-sheet distribution over the surface of the low-aspect-ratio triangular wing is pictured in figure 1(a). As the aspect ratio approaches zero the distribution of figure 1(a) becomes the simple two-dimensional fore and aft vortex distribution pictured in figure 1(b). Various wings having unswept trailing edges and approaching zero aspect ratio are pictured in figure 2. The vortex distributions of these wings are (similar to the wing of figure 1(a)) increasingly approximated by the two-dimensional vortex distribution of figure 1(b) as aspect ratio approaches zero. Hence, as aspect ratio approaches zero, the downwash normal to the wing, due to the vortex sheet of the wing, approaches that due to a two-dimensional vortex sheet. The plan-form boundary conditions that there be no flow through the plate can be easily satisfied by the two-dimensional vortex sheet because the downwash in the longitudinal direction is constant. The spanwise loading distribution is equal to the vortex strength distribution in the sheet.

From the linearized-compressible-flow equation, the aerodynamic characteristics of wings approach those given by zero aspect ratio as the wing nears the speed of sound. The compressibility equation requires that the longitudinal coordinate of a point in the plan form effectively increase as $1/\beta$. With this condition (referred to as the Prandtl transformation), wings approach zero aspect ratio in the same manner as those depicted in figure 2. Thus, at the speed of sound, plan forms having unswept trailing edges and moderate aspect ratios will also have their boundary conditions satisfied by the two-dimensional vortex sheet.

The two-dimensional vortex sheet can satisfy boundary conditions on the wing downstream from any chordwise angle-of-attack changes such as those due to control surfaces and camber. In the case of a localized change in angle of attack, the loading will actually be developed in a region near the bend in the wing surface, and in this region the boundary condition will not be satisfied by the simple two-dimensional vortex sheet. However, all loading changes that occur in any region of the wing are taken into account by the strength of the trailing vortex sheet, which must take up the configuration to satisfy the boundary conditions along the relatively infinite wing chord downstream. Thus, for wings of zero aspect ratio having unswept trailing edge, the loading depends only on the final angle of attack attained by the wing in the region of the trailing edge, provided the curvature of the wing chord is

small in ratio to the slope. The spanwise loading distribution is then independent of the chordwise location or distribution of a control-surface hinge line in the limiting case of zero aspect ratio or for moderate aspect ratio at the speed of sound. Also, for such wings, the total wing loading due to any chordwise distribution of camber depends only on the final angle of attack of the wing in the region of the trailing edge, provided the ratio of curvature to slope is small in this region.

Plan forms that approach zero aspect ratio by the Prandtl transformation, having other than an unswept trailing edge, can have the boundary condition satisfied by the two-dimensional vortex sheet, provided all points of the trailing edge remain at or behind the upstream line of maximum wing span. However, for these plan forms, the two-dimensional vortex sheet will only satisfy boundary conditions of chordwise changes in angle of attack that are at or ahead of a spanwise line through the maximum upstream point of the trailing edge. The reason for the limitation of wing plan forms is that the two-dimensional vortex sheet is applied to the full span of the wing and, if a trailing-edge indentation exists ahead of the upstream line of maximum span, part of the wing loading would be off the wing. The limitation for the chordwise changes in angle of attack is because, if a chordwise change in angle of attack with a resulting load change occurs aft of any point of the wing trailing edge, the application of the two-dimensional vortex-sheet boundary conditions as used herein would give wing loading off the wing. Figures 3(a) and 3(b) indicate the limitations for two plan forms. The spanwise loading is independent of chordwise change of angle of attack in the shaded area of figures 3(a) and 3(b), and depends only on the final angle of attack attained at the line through the maximum upstream point of the trailing edge. The theory limitations require that the angle of attack of the wing surface, which is not shaded in figures 3(a) and 3(b), remain equal to the angle of attack attained at the line bordering the two surface regions.

Figures 4(a) and 4(b) show swept wings approaching zero aspect ratio by modification of plan form in another way than that due to the Prandtl transformation. With the leading-edge sweep angle constant, the chord is assumed to approach infinity. The two-dimensional vortex sheet can satisfy the boundary conditions for all such wings if the aspect ratio is made small in such a way that the leading-edge angle remains constant and in the range $-\pi/2 > \Lambda_{L.E.} < \pi/2$.

In summation, the plan forms for which the boundary conditions are satisfied by the two-dimensional vortex sheet for zero-aspect-ratio wings, or moderate-aspect-ratio wings at the speed of sound, include:

1. All wings having an unswept trailing edge. (Spanwise loading is independent of chordwise angle-of-attack changes, depending only on the angle of attack of the trailing edge,

provided the curvature at the trailing edge is small compared with the slope. The control-surface hinge line can have any position on the wing chord.)

2. Those wings having swept trailing edge where every point of the trailing edge is at or behind the upstream line of maximum wing span. (For the plan-form region at or ahead of the spanwise line through the maximum forward position of the trailing edge, the spanwise loading is independent of chordwise angle-of-attack changes, depending only on the constant chordwise angle of attack of the region at or behind the spanwise line. The control-surface hinge line can have any position on the wing chord at or ahead of the spanwise line.)

The two-dimensional vortex theory employed herein is limited to unseparated flow, that is, flow that does not leave the wing surface along the chord. This requires that, for low aspect ratios, the aerodynamic angles be small. The extent that the aerodynamic results for control-surface hinge lines perpendicular to the air stream and blunt wings deviate from assumptions of the linearized-compressible-flow equation at the speed of sound is not known. However, the aerodynamic results from the linearized theory for these cases are included in the present report since the results are independent of plan form for the plan-form range considered. The spanwise loading is also independent of the chordwise location of the control-surface hinge line for low-aspect-ratio control surfaces.

Solution of Boundary Integral Equation

Downwash due to the two-dimensional vortex sheet.- The boundary condition that must be satisfied is that there be no flow through the surface of the airfoil. The downwash induced by the wing at, and normal to, the wing surface is thus equal to the upwash normal to the wing surface and experienced by the wing for a given angle-of-attack distribution and free-stream velocity.

The downwash due to a two-dimensional vortex sheet that extends to infinity fore and aft is given by

$$w(y) = \frac{1}{2\pi}\int_{-b/2}^{b/2} \frac{\Gamma'(\bar{y})}{y-\bar{y}}\, d\bar{y} \qquad (1)$$

With the assumption that the flow sticks to the wing plate, then the two-dimensional vortex sheet is at an angle of attack α and $w(y)$ is the induced velocity normal to the wing plate. The upwash normal to the wing

surface and experienced by the wing is equal to $V \sin \alpha(y)$ where $\alpha(y)$ is the spanwise angle-of-attack distribution. The boundary condition becomes

$$w(y) = V \sin \alpha(y) \tag{2}$$

With the dimensionless relations

$$G = \frac{\Gamma}{bV}, \quad \bar{\eta} = \frac{\bar{y}}{b/2}, \quad \eta = \frac{y}{b/2}$$

equation (1) becomes with equation (2) and for small values of $\alpha(y)$

$$\alpha(\eta) = \frac{1}{\pi} \int_{-1}^{1} \frac{G'(\bar{\eta})}{\eta - \bar{\eta}} \, d\bar{\eta} \tag{3}$$

Fourier series solution of equation (3).- Equation (3) gives the relation between the spanwise angle-of-attack distribution and the spanwise loading. Solution of the integral equation (3) for any spanwise distribution of angle of attack can give the vortex-strength distribution and thus the spanwise loading. The solution of equation (3) can be obtained by a method similar to those of wing-section and lifting-line theories.

The loading can be given by the trigonometric series

$$G(\varphi) = \sum_{n=1}^{\infty} a_n \sin n\varphi \tag{4}$$

then

$$G'(\varphi) = \sum_{n=1}^{\infty} n \, a_n \cos n\varphi \tag{5}$$

Equation (3) becomes with $\bar{\eta} = \cos \varphi$ and $\eta = \cos \varphi_\nu$

$$\alpha(\varphi_\nu) = \frac{1}{\pi}\int_0^\pi \frac{G'(\varphi)d\varphi}{\cos\varphi - \cos\varphi_\nu}$$

$$= \frac{1}{\pi}\sum_{n=1}^{\infty} n\, a_n \int_0^\pi \frac{\cos n\varphi}{\cos\varphi - \cos\varphi_\nu}\, d\varphi \qquad (6)$$

The following integral is derived in reference 5:

$$\int_0^\pi \frac{\cos n\varphi d\varphi}{\cos\varphi - \cos\varphi_\nu} = \frac{\pi \sin n\varphi_\nu}{\sin\varphi_\nu} \qquad (7)$$

Equations (6) and (7) give the solution of equation (3) as

$$\alpha(\varphi_\nu) = \sum_{n=1}^{\infty} \frac{n a_n \sin n\varphi_\nu}{\sin\varphi_\nu} \qquad (8)$$

Equation (8) relates the boundary conditions of the plan form with the unknown spanwise load distribution. The boundary conditions are that the upwash experienced by the plan form across the span, given by $\alpha(\varphi_\nu)$, equals the downwash created by the circulation given by the series. The solution of equation (8) requires only that values of a_n be found that are independent of φ_ν.

Equation (8) can be written as (omitting the subscript ν since φ_ν is continuous)

$$\alpha(\varphi)\sin\varphi = \sum_{n=1}^{\infty} n\, a_n \sin n\varphi \qquad (9)$$

which suggests the sine series of the Fourier series. The Fourier series for a function $f(\varphi)$ is given by

$$f(\varphi) = \sum_{n=1}^{\infty} B_n \sin n\varphi$$

where

$$B_n = \frac{1}{\pi} \int_0^{2\pi} f(\varphi) \sin n\varphi d\varphi \tag{10}$$

Let

$$na_n = B_n \tag{11}$$

then

$$a_n = \frac{1}{n\pi} \int_0^{2\pi} \alpha(\varphi) \sin \varphi \sin n\varphi d\varphi \tag{12}$$

The Fourier series repeats the function $f(\varphi)$ periodically for every 2π interval. In the present problem we are interested only in the interval from 0 to π; then equation (12) becomes

$$a_n = \frac{2}{n\pi} \int_0^{\pi} \alpha(\varphi) \sin \varphi \sin n\varphi d\varphi \tag{13}$$

With equation (13), the a_n values of the loading series given by equation (4) can be found for arbitrary angle-of-attack distribution.

Evaluation of a_n Coefficients

The spanwise loading series coefficients can be evaluated for any reasonable function $\alpha(\varphi)$. Functions $\alpha(\varphi)$ that produce additional loading due to constant angle of attack, loading due to rolling, basic loading due to twist for zero total lift, and spanwise loading due to control-surface deflection will be considered. The a_n coefficients that are determined can be inserted in equation (4) to obtain the spanwise loading distribution.

Additional loading.- For additional loading the upwash experienced by the wing is constant spanwise and equal to $V\alpha$, or $\alpha(\varphi) = \alpha$. Equation (13) gives

$$a_n = \frac{2\alpha}{n\pi} \int_0^{\pi} \sin \varphi \sin n\varphi d\varphi$$

then

$$\left.\begin{aligned} a_n &= \alpha \text{ for } n=1 \\ a_n &= 0 \text{ for } n\neq 1 \end{aligned}\right\} \tag{14}$$

Loading due to rolling.— For damping in roll the vertical velocity experienced by the wing is proportional to the distance from the wing midsection and the rate of roll, or equal to $-py = -V\,(pb/2V)\,\eta$, or $\alpha(\varphi) = -(pb/2V)\cos\varphi$. Equation (13) gives

$$a_n = \frac{-2(pb/2V)}{n\pi}\int_o^\pi \cos\varphi \sin\varphi \sin n\varphi d\varphi$$

then

$$\left.\begin{aligned} a_n &= \frac{-(pb/2V)}{4} \text{ for } n=2 \\ a_n &= 0 \text{ for } n\neq 2 \end{aligned}\right\} \tag{15}$$

Basic loading.— Basic loading is due to twist and/or spanwise change in camber where, for zero aspect ratio, the camber is the slope of the midcamber line at the region of the wing trailing edge. As distinguished from additional loading, the integral of the basic loading over the span is equal to zero, or $C_L = 0$. It will be shown that C_L is proportional to a_1 hence for $C_L = 0$; $a_1 = 0$. Equation (13) gives for $n=1$, and $a_1 = 0$.

$$\frac{2}{\pi}\int_o^\pi \alpha(\varphi) \sin^2\varphi\, d\varphi = 0 \tag{16}$$

Let

$$\alpha(\varphi) = \alpha_r + \epsilon(\varphi) \tag{17}$$

where α_r is the angle of attack of the wing root chord for $C_L = 0$, and $\epsilon(\varphi)$ is the wing twist relative to the wing root chord. Equation (17) in (16) gives

$$\alpha_r = -\frac{2}{\pi}\int_o^\pi \epsilon(\varphi) \sin^2\varphi\, d\varphi \tag{18}$$

With α_r constant, equation (13) becomes with $a_1 = 0$ for $n > 1$

$$a_n = \frac{2}{n\pi} \int_0^{\pi} \epsilon(\varphi) \sin \varphi \sin n\varphi d\varphi \tag{19}$$

The a_n coefficients for basic loading can be determined from equation (19) for arbitrary spanwise twist. The angle of attack of the wing root chord, for total lift equal to zero, is given by equation (18).

Basic loading due to linear twist.- All the possible variations of twist with span cannot be presented here. An example of the use of equations (18) and (19) for the case of linear washout or washin can readily be shown. For this case

$$\epsilon(\varphi) = \epsilon_o \left|\cos \varphi\right|$$

where ϵ_o is a constant giving the total twist at the wing tips relative to the root. A positive or negative value of ϵ_o gives washout or washin, respectively.

Equation (18) gives

$$\alpha_r = \frac{-4\epsilon_o}{\pi} \int_0^{\pi/2} \cos \varphi \sin^2 \varphi \, d\varphi = \frac{-4\epsilon_o}{3\pi} \tag{20}$$

Equation (19) gives

for $n > 1$

$$a_n = \frac{-2\epsilon_o}{n\pi} \left(\int_0^{\pi/2} \cos \varphi \sin \varphi \sin n\varphi d\varphi - \int_{\pi/2}^{\pi} \cos \varphi \sin \varphi \sin n\varphi d\varphi \right)$$

then

$$\left.\begin{aligned} a_n &= 0 \text{ for } n=2 \\ a_n &= \frac{-4\epsilon_o \sin (n\pi/2)}{\pi n(n^2-4)} \text{ for } n>2 \end{aligned}\right\} \tag{21}$$

Two arbitrary control surfaces.- Two control surfaces that can (1) have any position on the wing span, (2) have unlike control-surface spans, and (3) be deflected differently can be pictured as follows:

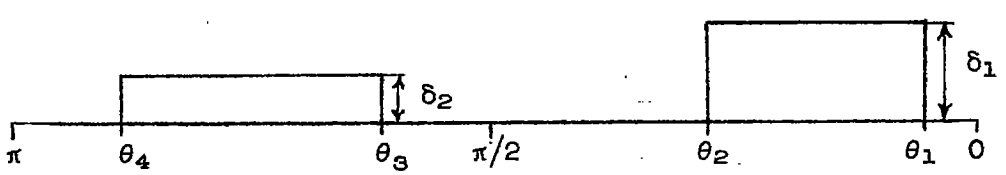

where θ's are arbitrary wing-span positions of the control-surface edges; and δ_1 and δ_2 are arbitrary control-surface deflections measured parallel to the plane of symmetry.

Then in equation (13)

$$\alpha(\varphi) = 0 \quad \text{from } \varphi=0 \quad \text{to } \theta_1$$

$$\alpha(\varphi) = \delta_1 \quad \text{from } \theta_1 \text{ to } \theta_2$$

$$\alpha(\varphi) = 0 \quad \text{from } \theta_2 \text{ to } \theta_3$$

$$\alpha(\varphi) = \delta_2 \quad \text{from } \theta_3 \text{ to } \theta_4$$

$$\alpha(\varphi) = 0 \quad \text{from } \theta_4 \text{ to } \pi$$

$$a_n = \frac{2\delta_1}{n\pi}\int_{\theta_1}^{\theta_2} \sin\varphi \sin n\varphi d\varphi + \frac{2\delta_2}{n\pi}\int_{\theta_3}^{\theta_4} \sin\varphi \sin n\varphi d\varphi$$

for $n=1$

$$a_1 = \frac{1}{\pi}\left\{\delta_1\left[\theta_2-\theta_1-\frac{1}{2}(\sin 2\theta_2-\sin 2\theta_1)\right] + \delta_2\left[\theta_4-\theta_3-\frac{1}{2}(\sin 2\theta_4-\sin 2\theta_3)\right]\right\}$$

for $n>1$

$$a_n = \frac{-2}{\pi n(n^2-1)}\left\{\delta_1\left[\cos\theta_1 \sin n\theta_1-\cos\theta_2 \sin n\theta_2 - n(\sin\theta_1 \cos n\theta_1-\sin\theta_2 \cos n\theta_2)\right] + \delta_2\left[\cos\theta_3 \sin n\theta_3-\cos\theta_4 \sin n\theta_4 - n(\sin\theta_3 \cos n\theta_3-\sin\theta_4 \cos n\theta_4)\right]\right\} \qquad (22)$$

Symmetric spanwise distribution of two control surfaces.– Two control surfaces distributed symmetrically on the wing span can be pictured as

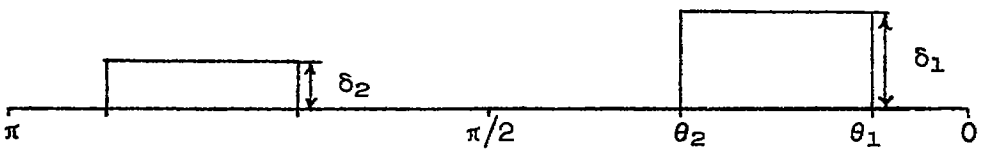

For this case

$$\theta_4 = \pi - \theta_1$$

$$\theta_3 = \pi - \theta_2$$

then equation (22) gives

for n=1

$$a_1 = \frac{\delta_1+\delta_2}{\pi}\left[\theta_2-\theta_1-\frac{1}{2}(\sin 2\theta_2-\sin 2\theta_1)\right]$$

for n>1

$$a_n = \frac{-2(\delta_1-\delta_2\cos n\pi)}{\pi n(n^2-1)}\left[\cos\theta_1\sin n\theta_1-\cos\theta_2\sin n\theta_2-n(\sin\theta_1\cos n\theta_1-\sin\theta_2\cos n\theta_2)\right] \qquad (23)$$

Inboard control surfaces.– Two inboard control surfaces of equal span can be pictured as

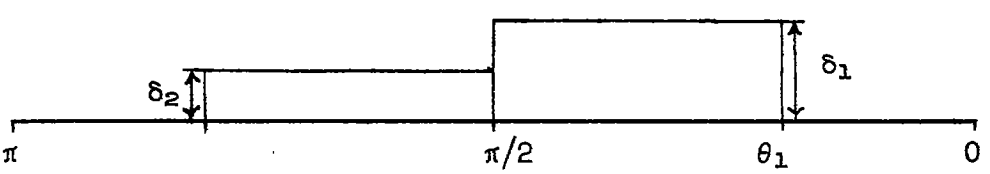

For this case $\theta_2 = \frac{\pi}{2}$ and equation (23) gives

for $n=1$

$$a_1 = \frac{(\delta_1+\delta_2)}{2\pi}(\pi-2\theta_1+\sin 2\theta_1)$$

for $n>1$

$$a_n = \frac{-2(\delta_1-\delta_2 \cos n\pi)}{\pi n(n^2-1)}\left(n \cos \frac{n\pi}{2} + \cos \theta_1 \sin n\theta_1 - n \sin \theta_1 \cos n\theta_1\right) \qquad (24)$$

Outboard control surfaces.- Two outboard control surfaces of equal span can be pictured as

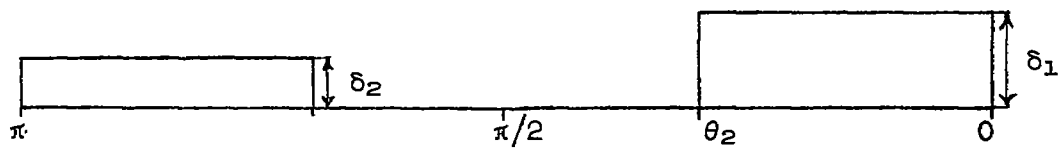

For this case $\theta_1=0$, and equation (23) gives

for $n=1$

$$a_1 = \frac{\delta_1+\delta_2}{2\pi}(2\theta_2-\sin 2\theta_2)$$

for $n>1$

$$a_n = \frac{2(\delta_1-\delta_2 \cos n\pi)}{\pi n(n^2-1)}\left(\cos \theta_2 \sin n\theta_2 - n \sin \theta_2 \cos n\theta_2\right) \qquad (25)$$

Aerodynamic Characteristics in Terms of the a_n Coefficients

In the foregoing sections the loading series coefficients were found for the several types of spanwise loading. In the following section aerodynamic characteristics will be found that are applicable to any of the loading series coefficient of the types of loadings considered.

The aerodynamic characteristics in terms of the a_n coefficients are tabulated as follows:

Loading distribution.—

$$G(\varphi) = \sum_{n=1}^{\infty} a_n \sin n\varphi \tag{4}$$

Lift coefficient.—

$$C_L = A \int_0^{\pi} G(\varphi) \sin \varphi \, d\varphi = \frac{\pi A}{2} a_1 \tag{26}$$

Rolling-moment coefficient.—

$$C_l = \frac{A}{2} \int_0^{\pi} G(\varphi) \sin \varphi \cos \varphi \, d\varphi = \frac{\pi A a_2}{8} \tag{27}$$

Induced drag coefficient.— To find the induced drag, use can be made of the principles of Munk (reference 6), in which the total induced drag is found by considering the inclination of the lift vector at an angle equal to one-half the ratio of the downwash in the wake to the free-stream velocity. The downwash angle in the wake is given by equation (8).

$$C_{D_i} = \frac{A}{2} \int_0^{\pi} G(\varphi) \alpha(\varphi) \sin \varphi \, d\varphi = \frac{\pi A}{4} \sum_{n=1}^{\infty} n a_n^2 \tag{28}$$

Semispanwise center of pressure for the right wing panel.—

$$\eta_{c.p.} = \frac{\int_0^{\frac{\pi}{2}} G(\varphi) \sin\varphi \cos\varphi \, d\varphi}{\int_0^{\frac{\pi}{2}} G(\varphi) \sin\varphi \, d\varphi} = \frac{\pi a_2 - 8 \sum_{\text{odd } n}^{\infty} \frac{(-1)^{\frac{n+1}{2}} a_n}{4-n^2}}{2\pi a_1 - 8 \sum_{\text{even } n}^{\infty} \frac{(-1)^{\frac{n}{2}} n a_n}{n^2-1}} \tag{29}$$

Semispanwise center of pressure for the left wing panel.—

$$\eta_{c.p.} = \frac{\int_{\frac{\pi}{2}}^{\pi} G(\varphi) \sin\varphi \cos\varphi \, d\varphi}{\int_{\frac{\pi}{2}}^{\pi} G(\varphi) \sin\varphi \, d\varphi} = \frac{\pi a_2 + 8 \sum_{\text{odd } n}^{\infty} \frac{(-1)^{\frac{n+1}{2}} a_n}{4-n^2}}{2\pi a_1 + 8 \sum_{\text{even } n}^{\infty} \frac{(-1)^{\frac{n}{2}} n a_n}{n^2-1}} \tag{30}$$

With equations (4) and (26) through (30) the loading distribution, lift coefficient, rolling moment, induced drag, and spanwise center of pressure can be found for additional, rolling, basic, or control-surface loadings considered in the previous section. For convenience, the equations giving the aerodynamic characteristics due to the various type loadings are tabulated in table I.

Relations for the Various Types of Loadings

Combination of the types of loadings.— The loading series coefficients are additive for various types of loading as implied by equation (13). The type of loading is determined by the angle-of-attack function, and summation of the angle-of-attack functions is equivalent to the summations of the loading series coefficients. Thus, all aerodynamic characteristics that depend linearly on the a_n coefficients are additive. As indicated by equations (4), (26), and (27), loading distribution, lift coefficient, and rolling moment are additive; whereas induced drag and center of pressure (equations (28), (29), and (30)) are not. To find induced drag and center of pressure for summations of

several types of loadings, the a_n coefficients can be added and induced drag and center of pressure recomputed with equations (28), (29), and (30) with the total a_n values.

Control-surface loading characteristics.- The slope of the loading distribution at any control-surface edge becomes infinite. From equation (4),

$$G'(\theta) = \sum_{n=1}^{\infty} n a_n \cos \theta$$

With any a_n of the control surfaces considered, $G'(\theta)$ contains a term of the type $\frac{\cos^2 n\theta}{n}$ which series diverges and sums to infinity. Thus, mathematically the loading distribution is vertical at these points; however, in plots of loading distribution this vertical slope is hardly discernible.

From the discussion of the previous section, the loading distribution for a given control-surface-angle distribution is additive with the loading for any other control-surface-angle distribution. As an example, this gives a simple relation between inboard and outboard flaps ($\delta_1=\delta_2$) for the same value of θ.

$$\left.\begin{aligned} G(\varphi)_{\text{outboard}} &= \delta \sin \varphi - G(\varphi)_{\text{inboard}} \\ \left(\frac{C_{L_\delta}}{A}\right)_{\text{outboard}} &= \frac{\pi}{2} - \left(\frac{C_{L_\delta}}{A}\right)_{\text{inboard}} \end{aligned}\right\} \qquad (31)$$

Closed function for loading series.- The spanwise loading distribution due to control-surface deflection is somewhat unwieldy in the series expansion. The infinite series can be summed to a closed function involving only elementary functions. The summation is mathematically detailed in the appendix together with the closed functions of the distributions of control surfaces considered.

Compressibility.- The equations of the present theory (tabulated in table I) can be multiplied through by β to give compressible parameters of aerodynamic coefficients and wing geometry. Then, subject to the limitations of the linearized-compressible-flow equation, the theory remains valid for low values of the parameter βA throughout the speed range. Thus, at sonic speeds for which β is small, aspect ratio can have moderate values.

RESULTS

Comparison With Other Theories

The present theory is in accord with the results of reference 1 for additional loading due to wing angle of attack as evaluated in table I. The additional loading lift coefficient and induced drag are identical with the results of reference 3 for the triangular wing at the speed of sound for any finite aspect ratio. Loading due to rolling and the damping-in-roll coefficient tabulated in table I as determined by the present theory are the same as that derived in reference 2 for the triangular wing of zero aspect ratio.

Reference 1 indicates that, in the low-aspect-ratio range, the aerodynamic characteristics dependent on spanwise loading vary much less with aspect ratio than do aerodynamic characteristics dependent on chordwise loading. In the present report the values of βC_{L_α} and βC_{l_p} deviate, due to increasing values of βA, from the results of other theories and are given for several plan forms by comparing the present theory with the subsonic theory of references 7 and 8 and shown in figures 5 and 6, respectively. Figures 7 and 8 give the comparative ranges of βC_{L_α} and βC_{l_p} as given by supersonic-theory values of references 9 and 10.

The range of βA that the present theory approximates can be judged by the use of figures 5 through 8, and all span loading characteristics that are given by the present theory in addition to C_{L_α} and C_{l_p} (e.g., C_{L_δ} and C_{l_δ} for control surfaces of low, compressible aspect ratio and full-wing-chord control surfaces) are expected to be equally accurate in this βA range. For supersonic speeds the plan form influences more strongly the range of βA approximated by the present theory. As seen in figures 7 and 8 only the pointed wings in supersonic flow asymptotically approach the present theory, while blunt wings approach the present theory more abruptly.

Figure Representation of Equations

The span loading distribution due to inboard or outboard flap deflection with no differential in the flap angles is given by letting $\delta_1 = \delta_2 = \delta_f$ in equations (24) and (25) and use of equation (4). Since the poor convergence of the span loading series for control surfaces requires that n be taken to the order of 30 for the order of accuracy shown in the plots, the closed function of the loading distribution given in the appendix and the relation between inboard and outboard flaps given by equation (31) saves considerable computing time. The symmetric spanwise loading due to inboard and outboard flap deflection is given in figures 9(a) and 10(a), respectively, for several flap spans. As presented, δ is measured parallel to the plane of symmetry.

For the limiting case of zero aspect ratio or at the speed of sound for moderate aspect ratio, G/δ_f is constant for any fraction of wing-chord control surface, provided the control surface itself is effectively of low aspect ratio.

The fact that spanwise loading is independent of the chordwise position of a control-surface hinge line is analogous to considering that the effective change of wing angle of attack to change of control-surface angle $d\alpha/d\delta$ is unity for all fractions of the wing chord. Since $d\alpha/d\delta$ is unity, the use of $d\alpha/d\delta$ has little significance for low-aspect-ratio control surfaces considered in the present report.

The loading distribution due to inboard or outboard aileron deflection with no differential between the ailerons is given by letting $\delta_1 = -\delta_2 = \delta_a$ in equations (24) and (25) and use of equation (4). The antisymmetric loading due to inboard or outboard aileron deflection is given by figures 9(b) and 10(b), respectively, for several aileron spans. Presented also in figure 10 is the loading distribution for additional loading and that due to rolling.

The induced drag coefficient of the wing due to inboard or outboard control surfaces is presented in figure 11 as a function of control-surface span.

The lift coefficient due to symmetrically deflected inboard or outboard flaps is given by letting $\delta_1 = \delta_2 = \delta_f$ in the respective equations of table I. Figure 12 gives the lift coefficient as a function of flap span and shows greater lift obtained with inboard flaps.

The rolling-moment coefficient due to antisymmetrically deflected inboard or outboard ailerons is given by letting $\delta_1 = -\delta_2 = \delta_a$ in the respective equations of table I. Figure 13 gives the rolling-moment coefficient as a function of aileron span and shows greater rolling moment obtained with outboard ailerons.

Basic loading depends on the twist of the wing. Camber is equivalent to twist if the slope of the mean camber line at the region of the trailing edge is considered as the twist angle. For linear washout or washin, twist as given by $\epsilon(\varphi) = \epsilon_o|\cos\varphi|$, the loading distribution given by the respective equation of table I is plotted in figure 14. The angle of twist at the wing tip given by ϵ_o is positive for washout and negative for washin.

CONCLUDING REMARKS

The theory developed herein will satisfactorily predict the span loading of low-aspect-ratio wings that have all points of the trailing

edge at or behind the upstream line of maximum span. The same results apply to moderate-aspect-ratio wings at the speed of sound wherever the principles of the linearized-compressible-flow theory are acceptable.

Application of the theory shows that the spanwise loading, such as additional loading due to angle of attack, that due to rolling, basic loading due to twist, and that due to arbitrary control surfaces of low aspect ratio, is independent of plan form for the range of wings considered.

For the plan forms having unswept trailing edges, the spanwise loading is independent of the chordwise position of the control surface and depends only on the slope of the trailing edge. The total loading due to camber depends only on the slope of the trailing edge, provided the curvature at the trailing edge is small compared with the slope.

For plan forms having swept trailing edge, the spanwise loading is independent of chordwise position of control surfaces, provided control-surface hinge line is at or ahead of a straight span line through the point of the maximum forward position of the trailing edge.

Ames Aeronautical Laboratory,
National Advisory Committee for Aeronautics,
Moffett Field, Calif., Aug. 15, 1949.

APPENDIX A

CLOSED FUNCTION FOR CONTROL SURFACE LOADING DISTRIBUTION

The spanwise loading distribution of the loading due to control surfaces can be put into a closed function. The loading distribution is given as the series

$$G(\varphi) = \sum_{n=1}^{\infty} a_n \sin n\varphi$$

where the a_n coefficients for the arbitrary control surface are given in equation (22).

Mathematics of the Series Summation

For a specified point θ at which a discontinuity in angle of attack occurs, the loading distribution is a function of two series given by

$$G(\varphi) = (\pm)\frac{\delta}{\pi}\left\{\left(\theta - \frac{1}{2}\sin 2\theta\right)\sin\varphi + 2\left[\cos\varphi \sum_{n=2}^{\infty} \frac{\sin n\theta \sin n\varphi}{n(n^2-1)} - \sin\theta \sum_{n=2}^{\infty} \frac{\cos n\theta \sin n\varphi}{n^2-1}\right]\right\} \tag{A1}$$

where the positive sign is taken for θ measured at the left edge of the wing section of angle of attack δ, and the negative sign for θ measured at the right edge of the wing section of angle of attack δ. In order to present $G(\varphi)$ as a closed function, the indicated two summations of equation (A1) must be made.

By the use of trigonometric identities the two infinite series of equation (A1) can be written, respectively, as

$$\frac{1}{2}\sum_{n=2}^{\infty} \frac{\cos n(\theta-\varphi)}{n(n^2-1)} - \frac{1}{2}\sum_{n=2}^{\infty} \frac{\cos n(\theta+\varphi)}{n(n^2-1)} \tag{A2}$$

and

$$\frac{1}{2}\sum_{n=2}^{\infty} \frac{\sin n(\theta+\varphi)}{n^2-1} - \frac{1}{2}\sum_{n=2}^{\infty} \frac{\sin n(\theta-\varphi)}{n^2-1} \tag{A3}$$

Let

$$z = e^{i\psi} = \cos\psi + i\sin\psi \tag{A4}$$

Then expressions (A2) and (A3) are the real and imaginary parts of the respective summations given by

$$\sum_{n=2}^{\infty} \frac{z^n}{n(n^2-1)} \tag{A5}$$

and

$$\sum_{n=2}^{\infty} \frac{z^n}{n^2-1} \tag{A6}$$

With the series, $\ln(1-z) = -\left(z + \frac{z^2}{2} + \ldots + \frac{z^n}{n} + \ldots\right)$

expression (A5) can be put into equivalent elementary functions by the following process:

$$\sum_{n=2}^{\infty} \frac{z^n}{n(n^2-1)} = \frac{1}{z} \int_0^z \int_0^z \sum_{n=2}^{\infty} \frac{z^{n-1}}{n-1}\, dz\,dz$$

$$= \frac{1}{z} \int_0^z \int_0^z \left[-\ln(1-z) \right] dz\,dz$$

$$= \frac{3z}{4} - \frac{1}{2} - \frac{(1-z)^2}{2z} \ln(1-z) \tag{A7}$$

Similarly, expression (A6) becomes

$$\sum_{n=2}^{\infty} \frac{z^n}{n^2-1} = \frac{1}{z} \int_0^z \sum_{n=2}^{\infty} \frac{z^n}{n-1}\, dz$$

$$= \frac{1}{z} \int_0^z \left[-z \ln (1-z) \right] dz$$

$$= \frac{1}{2} + \frac{z}{4} + \frac{1-z^2}{2z} \ln (1-z) \tag{A8}$$

With equation (A4) equations (A7) and (A8) become, respectively,

$$\sum_{n=2}^{\infty} \frac{z^n}{n(n^2-1)} = \frac{1}{4} + \left(2 \ln 2 \left|\sin \frac{\psi}{2}\right| - \frac{3}{2}\right) \sin^2 \frac{\psi}{2} + i\left(\frac{3}{4} \sin \psi + 2 \sin^2 \frac{\psi}{2} \cos^{-1} \sin \frac{\psi}{2}\right) \tag{A9}$$

and

$$\sum_{n=2}^{\infty} \frac{z^n}{n^2-1} = \frac{1}{4}(2 + \cos \psi) + \sin \psi \cos^{-1} \sin \frac{\psi}{2} + i (\sin \psi)\left(\frac{1}{4} - \ln 2 \left|\sin \frac{\psi}{2}\right|\right) \tag{A10}$$

The summations of expression (A2) are obtained by taking the real part of equation (A9) and are equal to

$$-\frac{1}{2}(1-\cos \theta \cos \varphi) \ln \left|\frac{\sin \frac{\theta+\varphi}{2}}{\sin \frac{\theta-\varphi}{2}}\right| - \frac{1}{2} \sin \theta \sin \varphi \ln \left|4\left(\sin \frac{\theta+\varphi}{2}\right)\left(\sin \frac{\theta-\varphi}{2}\right)\right| + \frac{3}{4} \sin \theta \sin \varphi \tag{A11}$$

The summations of expression (A3) are obtained by taking the imaginary part of equation (A10) and are equal to

$$\frac{1}{4} \cos \theta \sin \varphi - \frac{1}{2} \sin \theta \cos \varphi \ln \left|\frac{\sin \frac{\theta+\varphi}{2}}{\sin \frac{\theta-\varphi}{2}}\right| - \frac{1}{2} \cos \theta \sin \varphi \ln \left|4\left(\sin \frac{\theta+\varphi}{2}\right)\left(\sin \frac{\theta-\varphi}{2}\right)\right| \tag{A12}$$

The quantity within the brackets of eqaution (A1) is equal to the product of $\cos\theta$ and expression (A11) together with the product of $-\sin\theta$ and expression (A12). The loading distribution becomes

$$G(\varphi) = (\pm)\frac{\delta}{\pi}\left[\theta \sin\varphi + (\cos\varphi - \cos\theta)\ln\left|\frac{\sin\frac{\theta+\varphi}{2}}{\sin\frac{\theta-\varphi}{2}}\right|\right] \qquad (A13)$$

where, as before, the positive sign is taken for θ measured at the left edge of the wing section of angle of attack δ, and the negative sign for the right edge. Equation (A13) can be applied directly for the case of control surfaces considered in the text.

Two arbitrary control surfaces.–

$$G(\varphi) = \frac{\delta_1}{\pi}\left[(\theta_2-\theta_1)\sin\varphi + (\cos\varphi - \cos\theta_2)\ln\left|\frac{\sin\frac{\theta_2+\varphi}{2}}{\sin\frac{\theta_2-\varphi}{2}}\right| - (\cos\varphi - \cos\theta_1)\ln\left|\frac{\sin\frac{\theta_1+\varphi}{2}}{\sin\frac{\theta_1-\varphi}{2}}\right|\right] +$$

$$\frac{\delta_2}{\pi}\left[(\theta_4-\theta_3)\sin\varphi + (\cos\varphi - \cos\theta_4)\ln\left|\frac{\sin\frac{\theta_4+\varphi}{2}}{\sin\frac{\theta_4-\varphi}{2}}\right| - (\cos\varphi - \cos\theta_3)\ln\left|\frac{\sin\frac{\theta_3+\varphi}{2}}{\sin\frac{\theta_3-\varphi}{2}}\right|\right] \qquad (A14)$$

Symmetric spanwise distribution of two control surfaces.–

$$G(\varphi) = \frac{(\delta_1+\delta_2)}{\pi}(\theta_2-\theta_1)\sin\varphi \cdot \frac{\delta_1}{\pi}\left[(\cos\varphi - \cos\theta_2)\ln\left|\frac{\sin\frac{\theta_2+\varphi}{2}}{\sin\frac{\theta_2-\varphi}{2}}\right| - (\cos\varphi - \cos\theta_1)\ln\left|\frac{\sin\frac{\theta_1+\varphi}{2}}{\sin\frac{\theta_1-\varphi}{2}}\right|\right] +$$

$$\frac{\delta_2}{\pi}\left[(\cos\varphi + \cos\varphi_2)\ln\left|\frac{\cos\frac{\theta_2+\varphi}{2}}{\cos\frac{\theta_2-\varphi}{2}}\right| - (\cos\varphi + \cos\varphi_1)\ln\left|\frac{\cos\frac{\theta_1+\varphi}{2}}{\cos\frac{\theta_1-\varphi}{2}}\right|\right] \qquad (A15)$$

Inboard control surfaces.—

$$G(\varphi) = \left(\frac{\delta_1+\delta_2}{\pi}\right)\left(\frac{\pi}{2}-\theta_1\right)\sin\varphi +$$

$$\frac{\delta_1}{\pi}\left[\cos\varphi \ln\left|\frac{1+\sin\varphi}{\cos\varphi}\right| - (\cos\varphi-\cos\theta_1)\ln\left|\frac{\sin\frac{\theta_1+\varphi}{2}}{\sin\frac{\theta_1-\varphi}{2}}\right|\right] +$$

$$\frac{\delta_2}{\pi}\left[\cos\varphi \ln\left|\frac{1-\sin\varphi}{\cos\varphi}\right| - (\cos\varphi+\cos\theta_1)\ln\left|\frac{\cos\frac{\theta_1+\varphi}{2}}{\cos\frac{\theta_1-\varphi}{2}}\right|\right] \quad (A16)$$

Outboard control surfaces.—

$$G(\varphi) = \frac{(\delta_1+\delta_2)}{\pi}\theta_2\sin\varphi +$$

$$\frac{\delta_1}{\pi}(\cos\varphi-\cos\theta_2)\ln\left|\frac{\sin\frac{\theta_2+\varphi}{2}}{\sin\frac{\theta_2-\varphi}{2}}\right| +$$

$$\frac{\delta_2}{\pi}(\cos\varphi+\cos\theta_2)\ln\left|\frac{\cos\frac{\theta_2+\varphi}{2}}{\cos\frac{\theta_2-\varphi}{2}}\right| \quad (A17)$$

REFERENCES

1. Jones, Robert T.: Properties of Low-Aspect-Ratio Pointed Wings at Speeds Below and Above the Speed of Sound. NACA Rep. 835, 1946.

2. Ribner, Herbert S.: The Stability Derivatives of Low-Aspect-Ratio Triangular Wings at Subsonic and Supersonic Speeds. NACA TN 1423, 1947.

3. Heaslet, Max. A., Lomax, Harvard, and Spreiter, John R.: Linearized Compressible-Flow Theory for Sonic Flight Speeds. NACA TN 1824, 1949.

4. Bollay, William: A Theory for Rectangular Wings of Small Aspect Ratio. Jour. Aero. Sci., vol. 4, no. 7, May 1937, pp. 294–296.

5. Durand, W. F.: Aerodynamic Theory. Berlin, J. Springer, 1934. vol. II, pp. 173–174.

6. Munk, Max M.: The Minimum Induced Drag of Aerofoils. NACA Rep. 121, 1921.

7. DeYoung, John: Theoretical Additional Span Loading Characteristics of Wings with Arbitrary Sweep, Aspect Ratio, and Taper Ratio. NACA TN 1491, 1947.

8. Bird, John D.: Some Theoretical Low-Speed Span Loading Characteristics of Swept Wings in Roll and Sideslip. NACA TN 1839, 1949.

9. Puckett, A. E., and Stewart, H. J.: Aerodynamic Performance of Delta Wings at Supersonic Speeds. Jour. of Aero. Sci., vol. 14, no. 10, Oct. 1947, pp. 567–578.

10. Jones, Arthur L., and Alksne, Alberta: The Damping Due to Roll of Triangular, Trapezoidal, and Related Plan Forms in Supersonic Flow. NACA TN 1548, 1948.

TABLE I.– EQUATIONS FOR VARIOUS AERODYNAMIC CHARACTERISTICS

Reference equation	[1]$c_l(\varphi)$ spanwise loading distribution	C_L	C_l	C_{D_i}
		Additional loading		
(14)	$\alpha \sin\varphi$, $\eta_{c.p.} = \frac{4}{3\pi}$	$\frac{\pi A}{2}\alpha$	0	$\frac{\pi A}{4}\alpha^2$
		Loading due to rolling		
(15)	$\frac{-(pb/2V)}{4}\sin 2\varphi$, $\eta_{c.p.} = \frac{3\pi}{16}$	0	$-\frac{\pi A}{32}\left(\frac{pb}{2V}\right)$	$\frac{\pi A}{32}\left(\frac{pb}{2V}\right)^2$
		Basic loading		
(19)	$\sum_{n=2}^{\infty} a_n \sin n\varphi$ $a_n = \frac{2}{n\pi}\int_0^{\pi} \epsilon(\varphi)\sin\varphi \sin n\varphi d\varphi$	For $C_L = 0$ $\alpha_r = -\frac{2}{\pi}\int_0^{\pi}\epsilon(\varphi)\sin^2\varphi d\varphi$	$\frac{\pi A a_2}{8}$	$\frac{\pi A}{4}\sum_{n=2}^{\infty} n a_n^2$
		Basic loading due to linear twist		
(21)	$\frac{4\epsilon_0}{\pi}\sum_{n=3,5,7}^{\infty}\frac{(-1)^{\frac{n-1}{2}}\sin n\varphi}{n(n^2-4)}$ (where ϵ_0 is positive for washout, negative for washin)	For $C_L = 0$ $\alpha_r = -\frac{4\epsilon_0}{3\pi}$	0	$\frac{4\pi A\epsilon_0^2}{\pi}\sum_{n=3,5,7}^{\infty}\frac{1}{n(n^2-4)^2}$
		Loading due to two arbitrary control surfaces[2]		
(22) [3](A14)	$\sum_{n=1}^{\infty} a_n \sin n\varphi$	$\frac{A\delta_1}{2}\left[\theta_2-\theta_1-\frac{1}{2}(\sin 2\theta_2-\sin 2\theta_1)\right]+$ $\frac{A\delta_2}{2}\left[\theta_4-\theta_3-\frac{1}{2}(\sin 2\theta_4-\sin 2\theta_3)\right]$	$\frac{A\delta_1}{12}(\sin^3\theta_2-\sin^3\theta_1)+$ $\frac{A\delta_2}{12}(\sin^3\theta_4-\sin^3\theta_3)$	$\frac{\pi A}{4}\sum_{n=1}^{\infty} n a_n^2$
		Loading due to symmetric distribution of two control surfaces		
(23) [3](A15)	$\sum_{n=1}^{\infty} a_n \sin n\varphi$	$\frac{A}{2}(\delta_1+\delta_2)\left[\theta_2-\theta_1-\frac{1}{2}(\sin 2\theta_2-\sin 2\theta_1)\right]$	$\frac{A}{12}(\delta_1-\delta_2)(\sin^3\theta_2-\sin^3\theta_1)$	$\frac{\pi A}{4}\sum_{n=1}^{\infty} n a_n^2$
		Loading due to inboard control surfaces		
(24) [3](A16)	$\sum_{n=1}^{\infty} a_n \sin n\varphi$	$\frac{A}{4}(\delta_1+\delta_2)(\pi-2\theta_1+\sin 2\theta_1)$	$\frac{A}{12}(\delta_1-\delta_2)(1-\sin^3\theta_1)$	$\frac{\pi A}{4}\sum_{n=1}^{\infty} n a_n^2$
		Loading due to outboard control surfaces		
(25) [3](A17)	$\sum_{n=1}^{\infty} a_n \sin n\varphi$	$\frac{A}{4}(\delta_1+\delta_2)(2\theta_2-\sin 2\theta_2)$	$\frac{A}{12}(\delta_1-\delta_2)\sin^3\theta_2$	$\frac{\pi A}{4}\sum_{n=1}^{\infty} n a_n^2$

[1]The spanwise center of pressure for the right and left wing panels is given by equations (29) and (30).

[2]θ_1 and θ_4 give the wing span position (cos θ) of the outboard edges of the control surfaces; θ_2 and θ_3 denote the inboard edges.

[3]Closed functions for the spanwise loading distribution of control surfaces are given in the appendix.

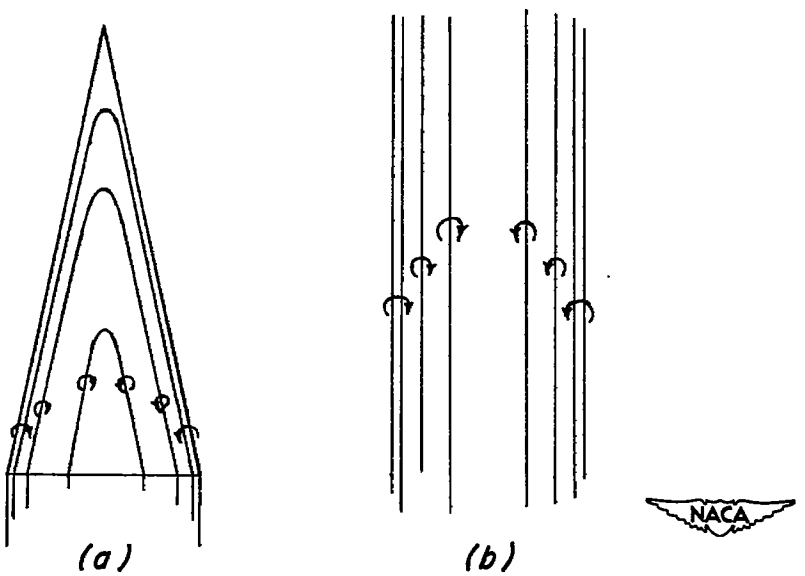

Figure 1.— Vortex sheet of low-aspect-ratio wing and corresponding approximate two-dimensional vortex sheet.

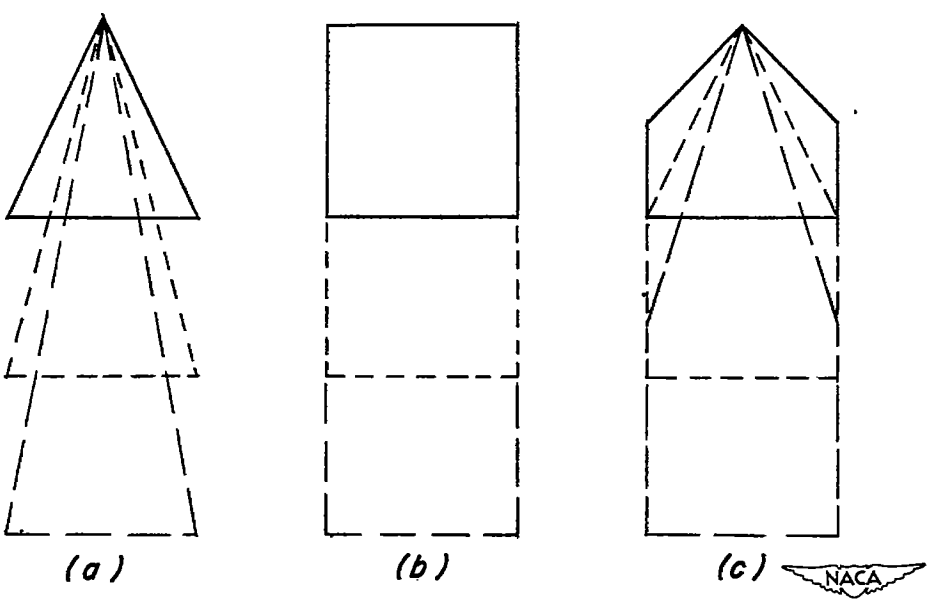

Figure 2.— Plan forms having unswept trailing edges approaching zero aspect ratio by increasing longitudinal coordinates of plan forms.

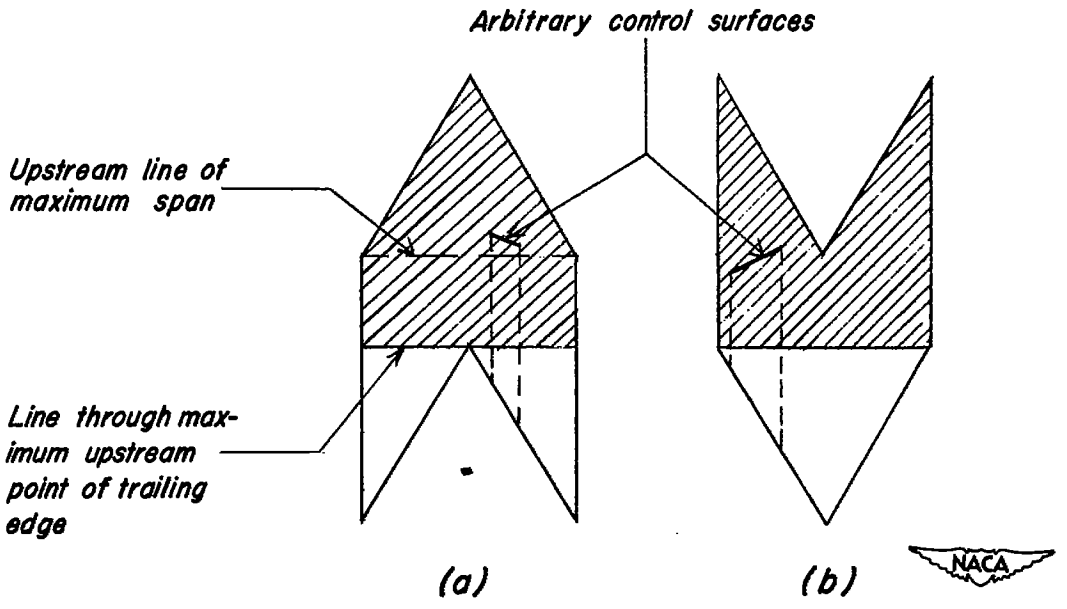

Figure 3.— Plan forms having swept trailing edge showing shaded regions where chordwise variations of angle of attack are permissible in the present analysis.

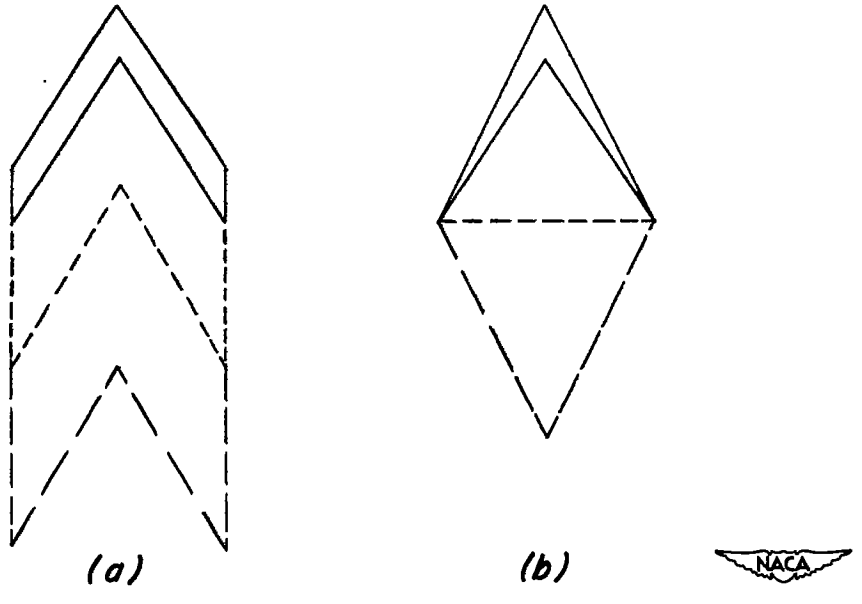

Figure 4.— Plan forms approaching zero aspect ratio that maintain a constant leading-edge sweep angle.

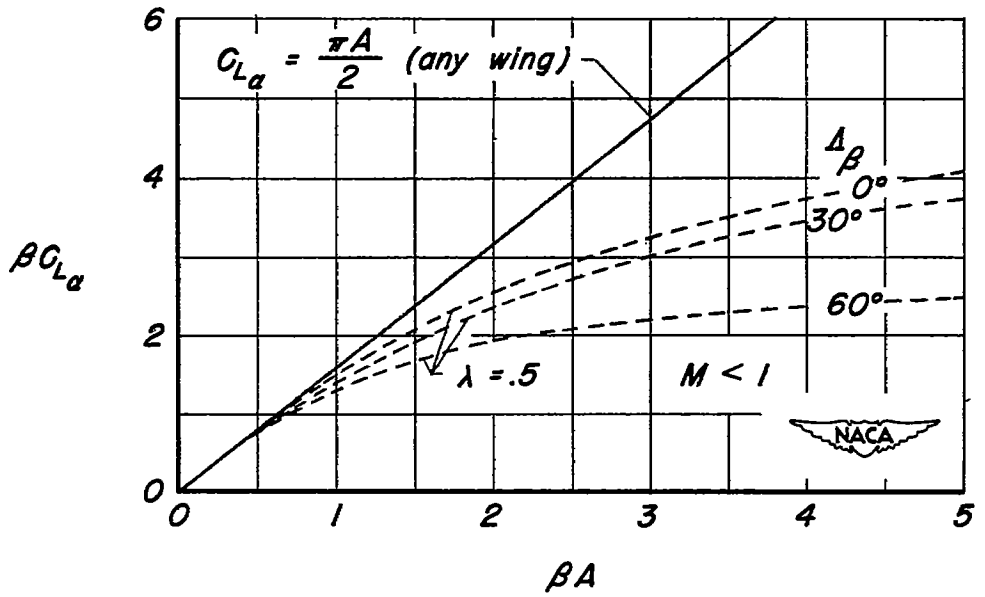

Figure 5.- Comparison of lift-curve-slope parameter, βC_{L_α}, with calculations of reference 7.

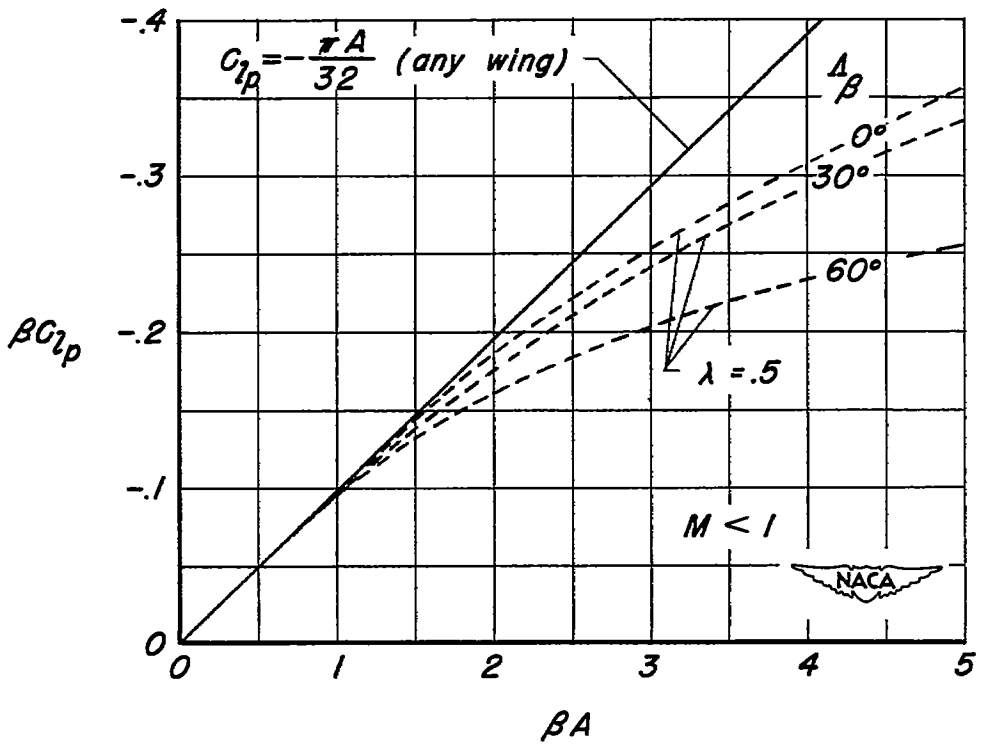

Figure 6.- Comparison of damping-in-roll parameter, βC_{l_p}, with calculations of reference 8.

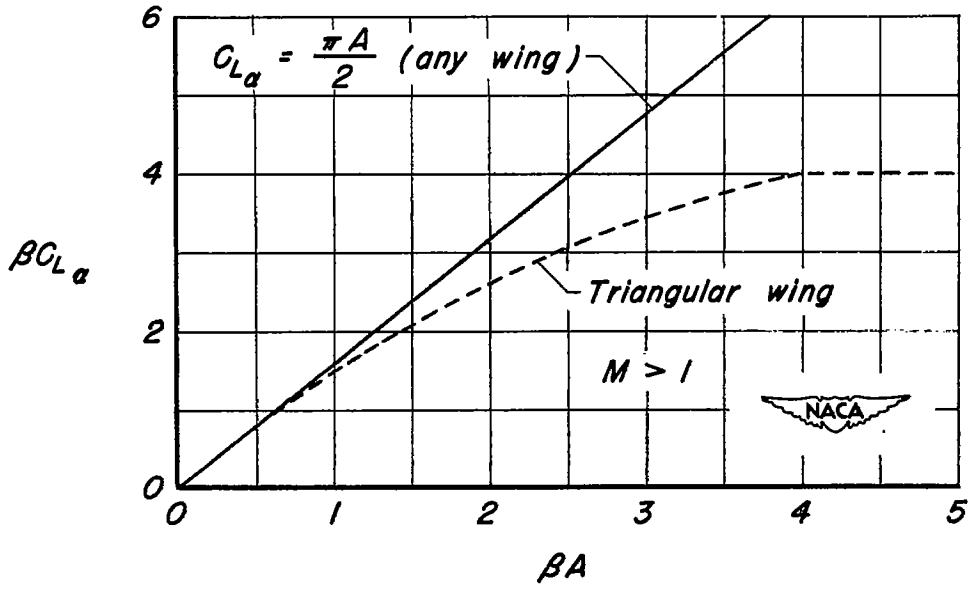

Figure 7.—Comparison of lift-curve-slope parameter, βC_{L_α}, with calculations of reference 9.

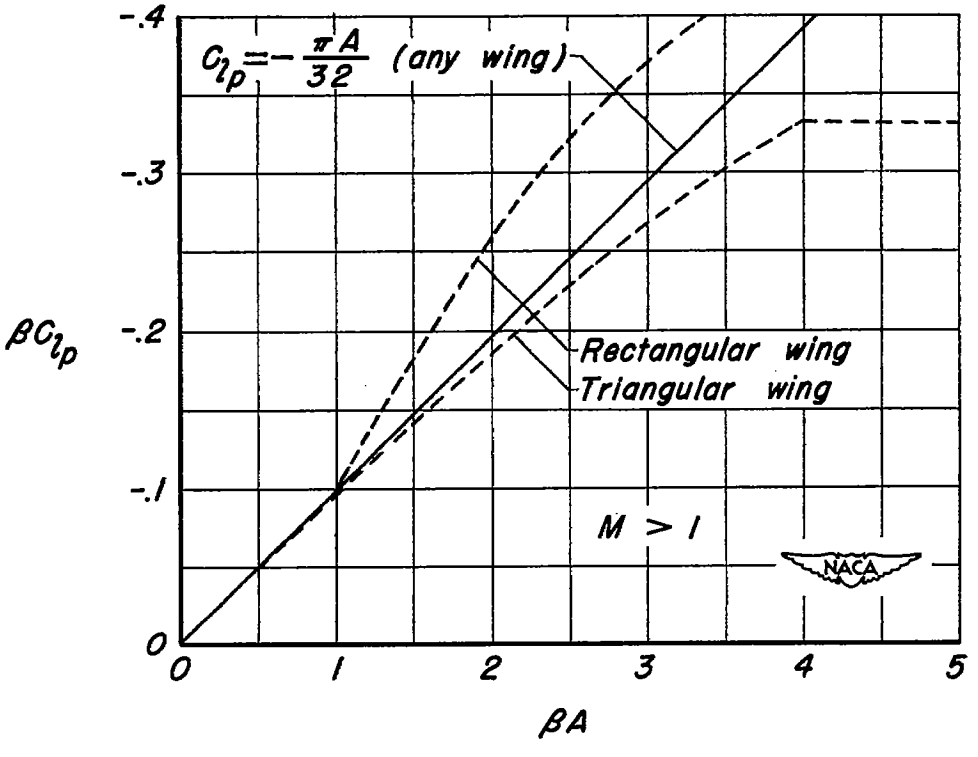

Figure 8.—Comparison of damping-in-roll parameter, βC_{l_p}, with calculations of reference 9.

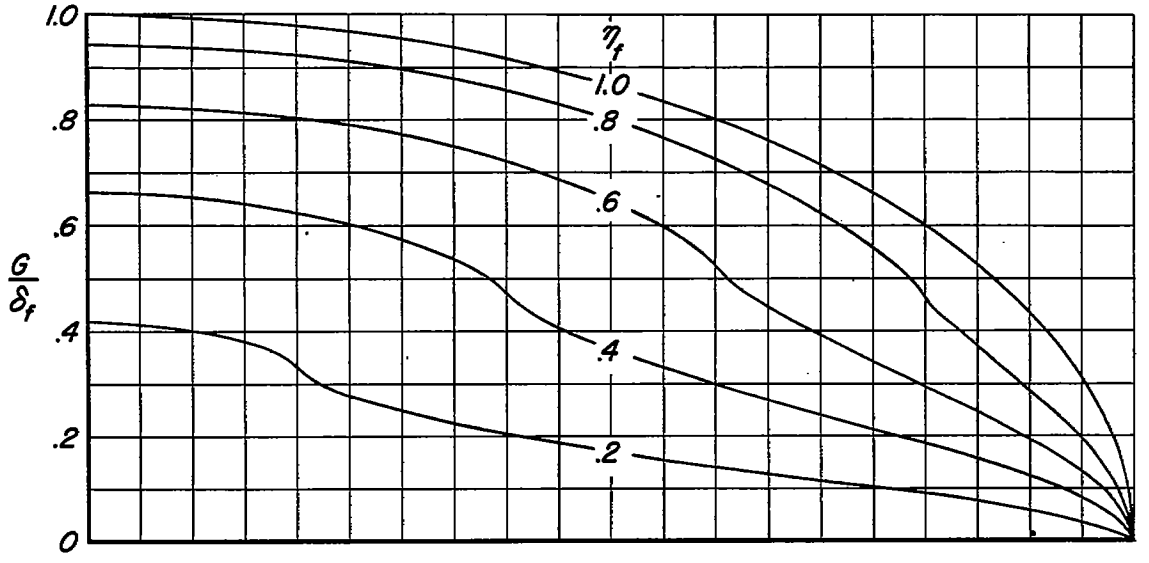

(a) Symmetric flap deflection.

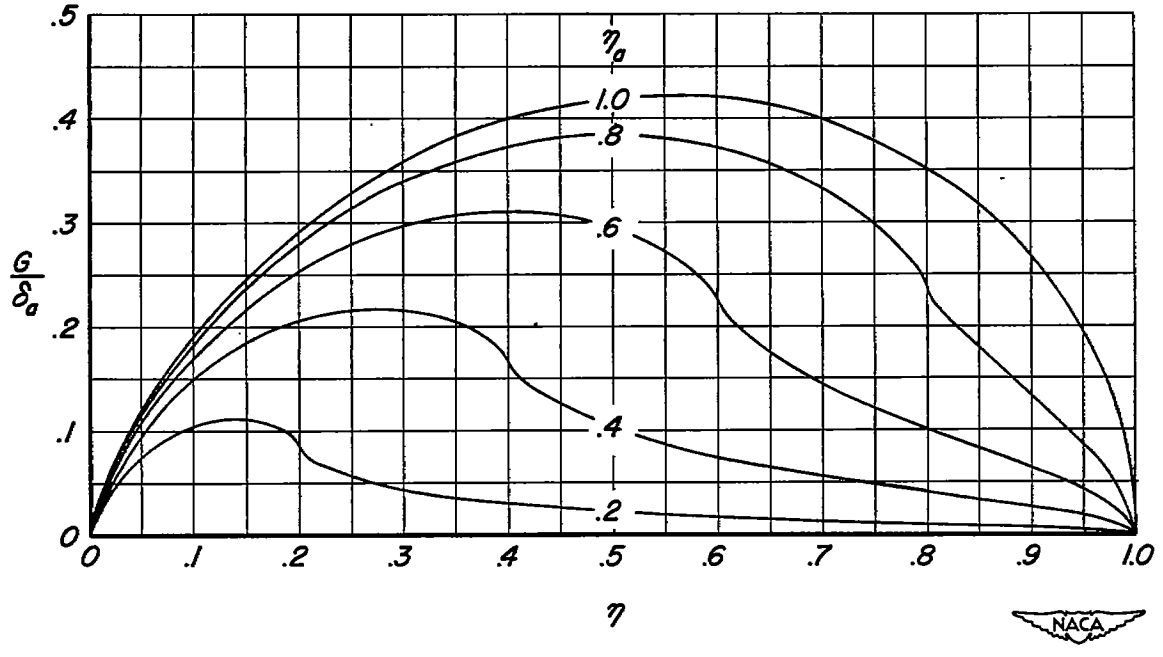

(b) Antisymmetric aileron deflection.

Figure 9.- Wing semispan loading distribution, per radian, due to inboard control surfaces for various control-surface spans.

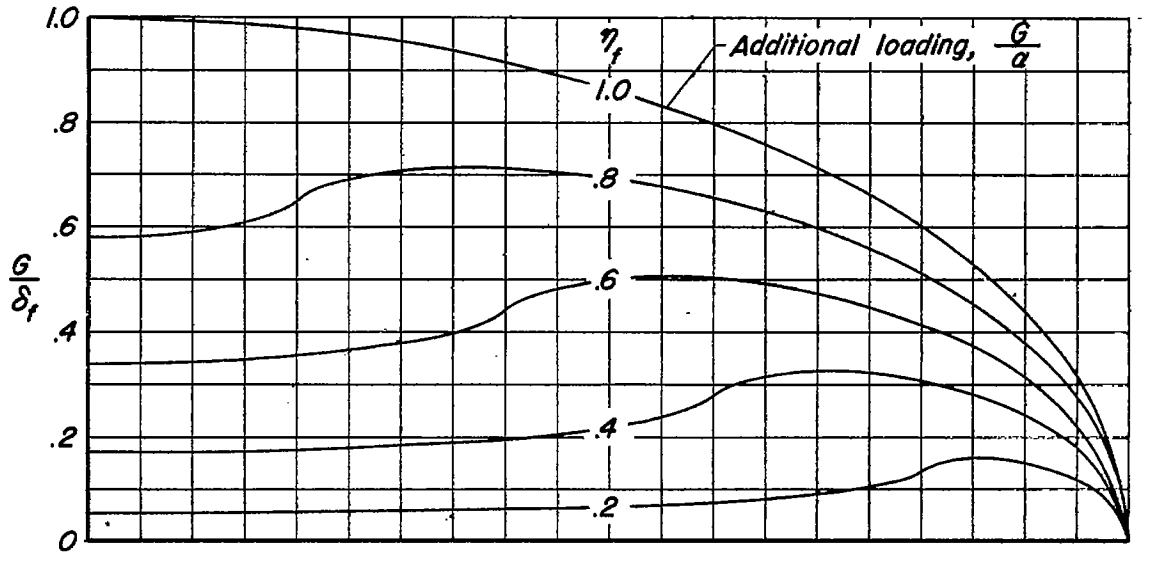

(a) Symmetric flap deflection.

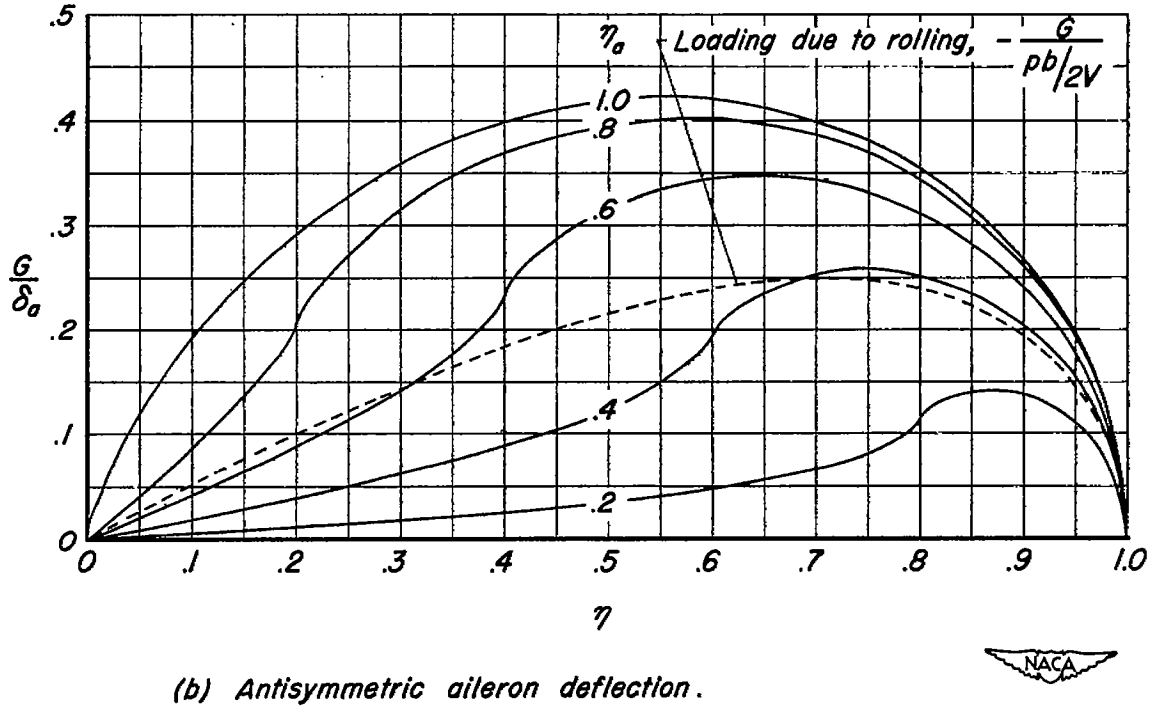

(b) Antisymmetric aileron deflection.

Figure 10.- Wing semispan loading distribution, per radian, due to outboard control surfaces for various control-surface spans.

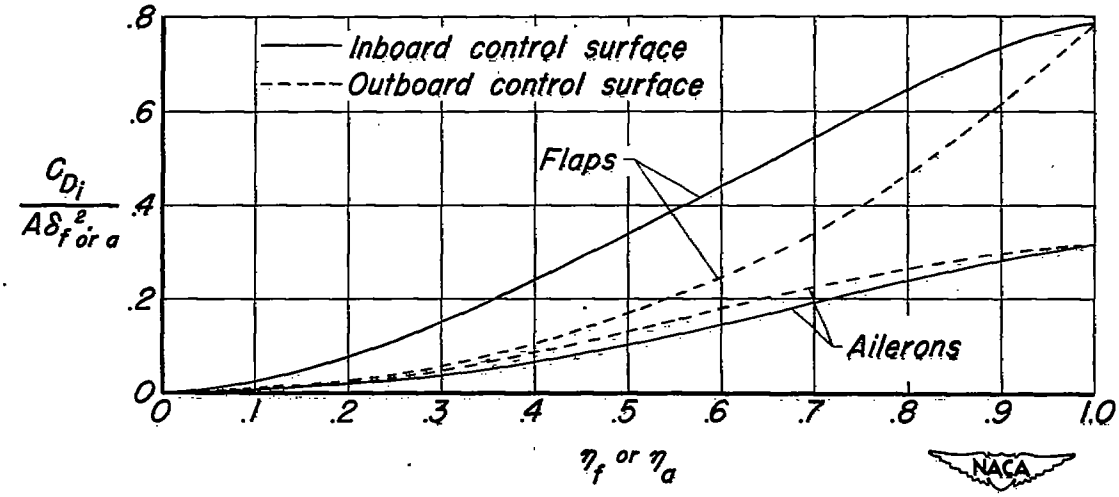

Figure 11.- Induced drag, per radian squared, due to symmetrically deflected flaps or antisymmetrically deflected ailerons as a function of control-surface span.

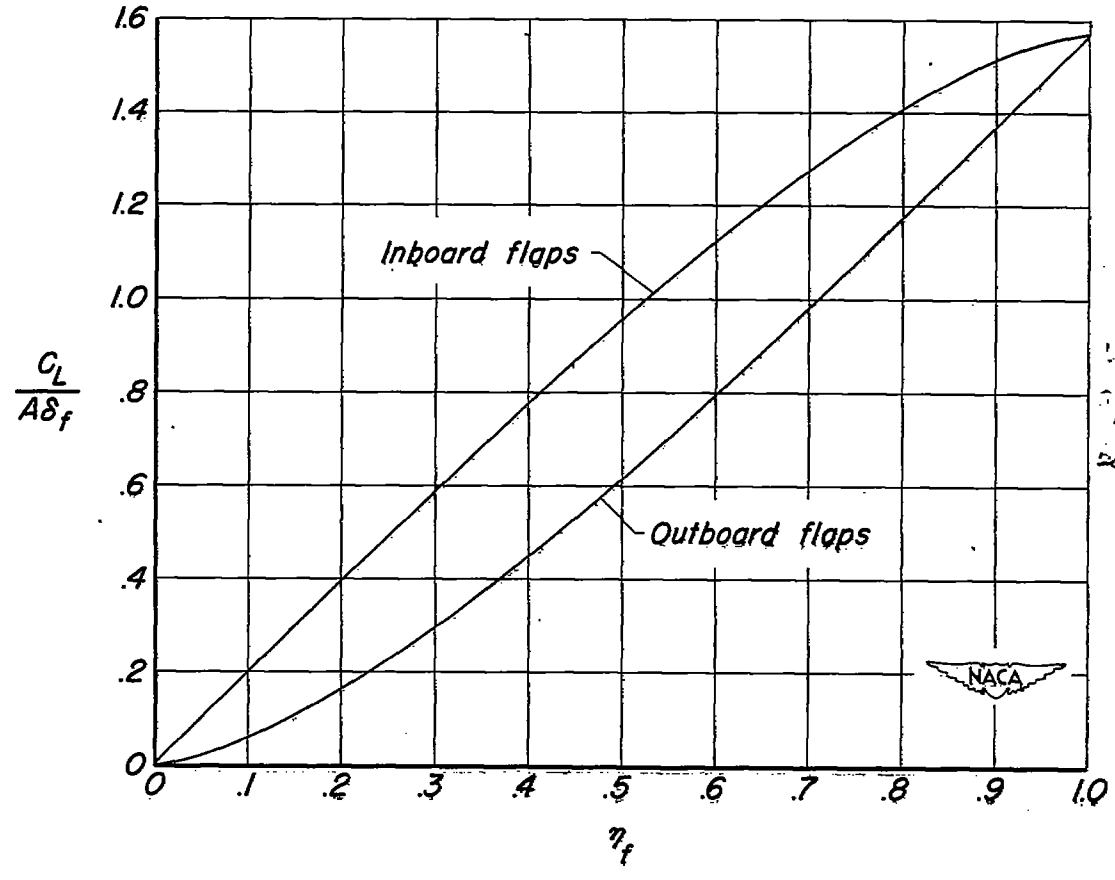

Figure 12.- Comparative lift, per radian, due to symmetrically deflected inboard or outboard flaps as a function of flap span.

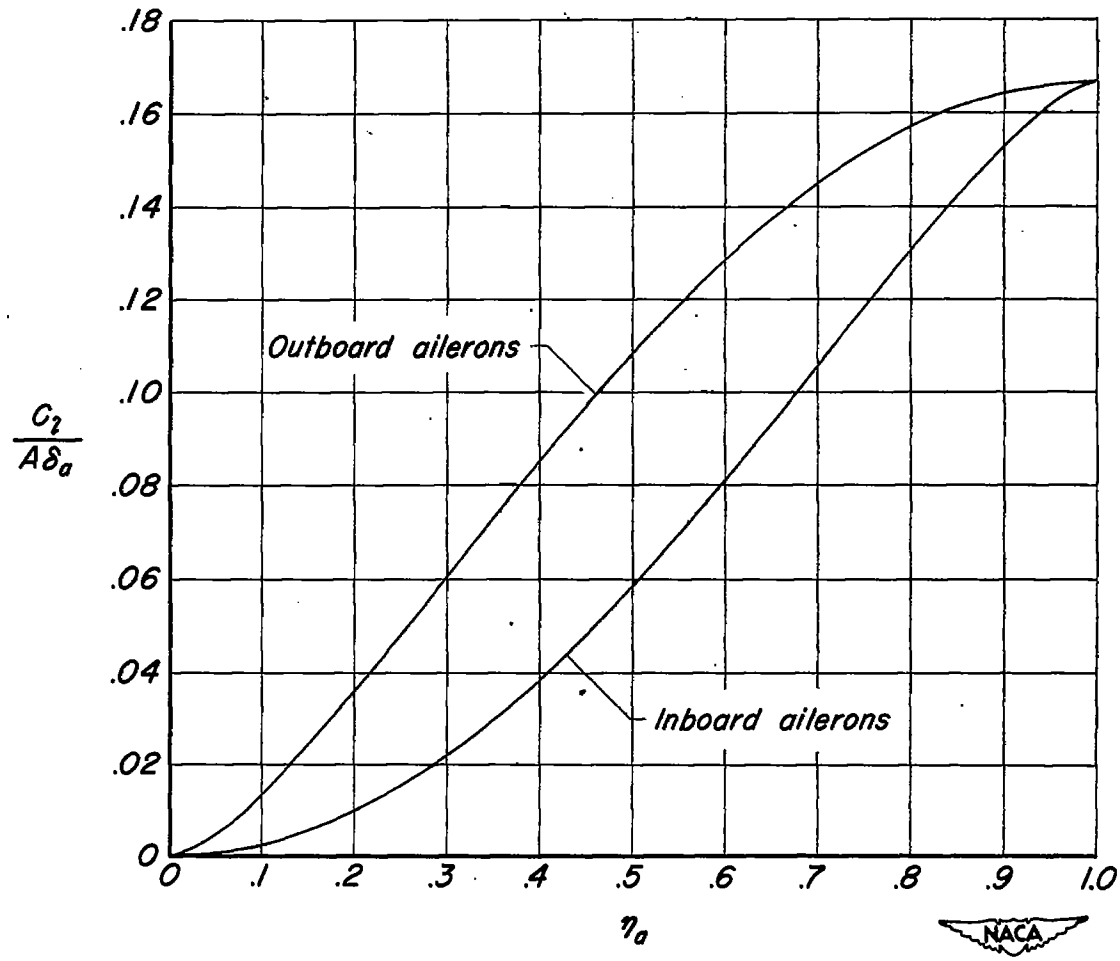

Figure 13.- Comparative rolling moment, per radian, due to antisymmetrically deflected inboard or outboard ailerons as a function of aileron span.

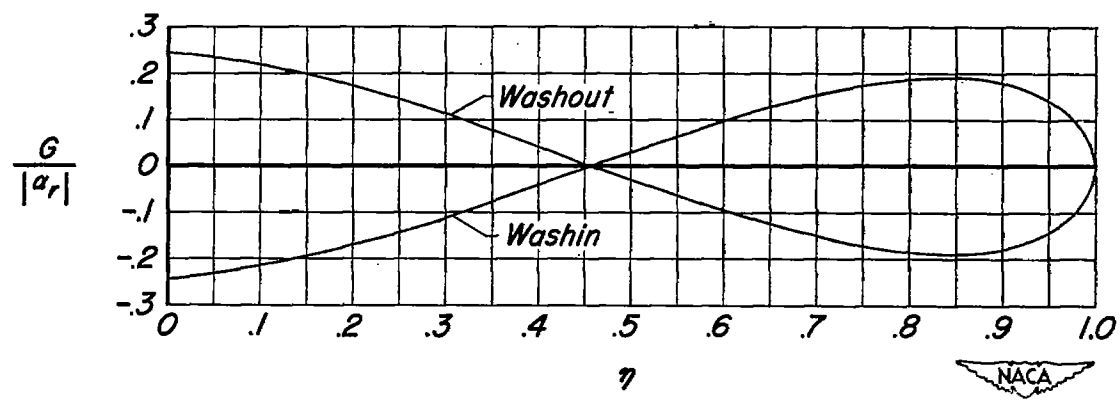

Figure 14.- Wing semispan loading distribution, per radian, for wings with symmetric linear twist, $\pm \epsilon_o = \mp \frac{3\pi}{4} a_r$.